Glass transition in thin supported polystyrene films probed by temperature-modulated ellipsometry in vacuum

Mikhail Yu. Efremov,[*] Anna V. Kiyanova, Julie Last, Shauheen S. Soofi, Christopher Thode, and Paul F. Nealey
Department of Chemical and Biological Engineering and Center for Nanotechnology, University of Wisconsin–Madison, Madison, Wisconsin 53706, USA

(Received 27 April 2012; published 7 August 2012)

Glass transition in thin (1–200 nm thick) spin-cast polystyrene films on silicon surfaces is probed by ellipsometry in a controlled vacuum environment. A temperature-modulated modification of the method is used alongside a traditional linear temperature scan. A clear glass transition is detected in films with thicknesses as low as 1–2 nm. The glass transition temperature (T_g) shows no substantial dependence on thickness for coatings greater than 20 nm. Thinner films demonstrate moderate T_g depression achieving 18 K for thicknesses 4–7 nm. Less than 4 nm thick samples are excluded from the T_g comparison due to significant thickness nonuniformity (surface roughness). The transition in 10–20 nm thick films demonstrates excessive broadening. For some samples, the broadened transition is clearly resolved into two separate transitions. The thickness dependence of the glass transition can be well described by a simple 2-layer model. It is also shown that T_g depression in 5 nm thick films is not sensitive to a wide range of experimental factors including molecular weight characteristics of the polymer, specifications of solvent used for spin casting, substrate composition, and pretreatment of the substrate surface.

DOI: 10.1103/PhysRevE.86.021501 PACS number(s): 64.70.pj, 68.60.Dv, 78.66.Qn

I. INTRODUCTION

Evaluation of glass transition parameters in thin films continues to be a well-explored topic in the actively developing field of *nanometrology* (characterization of nanometers-sized objects). The dependence of the glass transition temperature (T_g) on film thickness in the model system of thin supported polystyrene (PS) films has attracted extraordinary attention [1–12]. T_g values in thin PS films have been measured by many research groups employing varying experimental techniques. The results span significant (tens of degrees) T_g depression on the order of 10 nm thick coatings [12–15] to an independence of T_g on thickness [8,16–18] and further to substantial T_g increase in thin films [19,20].

The experimental challenges encountered by researchers in the field have initiated numerous advances in the related instrumentation, experimental design, and data processing [8,21]. Particular attention has been paid to the factors that play a significant role in the thinnest films but become negligible with increased film thickness. New trends in this area include, but are not limited to, using a controlled environment that limits sorption of water on the film interfaces [22,23] and polymer oxidation at elevated temperatures [24], improving the sensitivity of techniques [25], and employing more sophisticated data analysis methods [21].

In this work we demonstrate that the *de facto* standard technique for the field, ellipsometry, enhanced by state-of-the-art experimental practices can resolve layer-dependent dynamics in thin coatings. Not only can T_g be more accurately determined, but the details of the relaxation dynamics, such as the width and fine structure of the transition, are also readily achievable by the technique. The thickness dependence of these parameters can be used for probing the dynamics at different depths of a sample film.

Models that assume stratification of the coatings, where each layer is characterized by specific dynamics, have been proposed in the early works on glass transition in confinement [19,26,27] and have since gained wide acceptance [3,5,28]. In general, there are two ways to probe the distribution of the dynamics across thin films—direct probe of each layer and interpretation of the film behavior in respect of thickness [3]. In the pioneering work by Ellison and Torkelson [29], the direct probe of the glass transition in a selected layer was achieved by labeling of the layer with a fluorescent marker sensitive to the polymer dynamics. Ellipsometry, the technique of choice for this work, exemplifies the second approach—inferring of the layer properties from the global film behavior. Despite being indirect in this sense, ellipsometry has many other advantages. As a member of the large group of "dilatometric" methods, ellipsometry provides comparable results with many other techniques that probe thermal expansion of the film [30]. Importantly, ellipsometry is a nondestructive and markerless technique. The absence of mandatory impurities (markers, labels, or probes) prevents complications such as altering of the polymer matrix properties, probe segregation, and redistribution [30–32]. In addition, both controlled and vacuum environments are compatible with ellipsometric measurements [23]. This work presents a good illustration of how a layered model of glassy dynamics in a thin polymer film can be dependably derived using advanced ellipsometric techniques.

II. EXPERIMENTAL SECTION

A. Ellipsometry in vacuum

The ellipsometry technique used to probe glass transition in thin supported PS films is described in detail elsewhere [23]. Temperature modulation (TM) modification of the ellipsometry setup is introduced and discussed in our previous work [33].

[*]To whom correspondence should be addressed; efremov@wisc.edu

 ©2012 American Physical Society

Briefly, the experimental setup is based on a custom-built spectroscopic phase-modulated ellipsometer and an optical vacuum chamber equipped with a variable temperature sample holder. Configuration of the ellipsometer ensures high sensitivity for thin films on a bare silicon surface. Extensive data accumulation further increases the signal-to-noise ratio. The temperature program includes both heating and cooling runs in the 20–160 °C range. Temperature modulation for both heating and cooling programs helps to filter out irreversible thermal processes that can mask the glass transition. A linear temperature program is used for comparison with TM scans and when a better temperature resolution of thermal changes is required. During scans, the ellipsometric angle Δ is recorded for one selected wavelength (504 nm). At shorter wavelengths the signal starts to degrade due to the increased scattering of the probing light; longer wavelengths correspond to decreased sensitivity to the sample thickness changes. A typical experimental procedure consists of 3 TM scan cycles (heating and cooling) followed by 21 linear scan cycles. The temperature program includes *in situ* annealing of the sample after the first TM heating scan at 160 °C for 6 h. After all other heating scans, hour-long isothermal steps at 160 °C are inserted into the program to facilitate erasing the thermal history of the sample. The linear scan records are analyzed for outliers and averaged to reduce noise. Scan rates for linear and TM scans are 1 K/min and 0.1 K/min, respectively. A typical TM period is 10 min. Typical examples of individual $\Delta(T)$ linear scan records (raw data) are given in the Supplemental Material [34].

For all investigated samples Δ is a smooth monotonic function of film thickness. During the temperature runs, the thickness changes only by a small fraction (a few %). Consequently, for each experiment the dependence of Δ on thickness can be well approximated by a linear function. Considering thermal expansion process only, the derivative $d\Delta/dT$ is practically proportional to the thermal coefficient of film expansion. Final records are presented in the form of $d\Delta/dT(T)$ functions. On the $d\Delta/dT$ vs temperature plots, the glass transition is manifested by a step between straight line segments representing the glassy and liquid states. Glass transition temperature T_g is assigned using the limiting fictive temperature (T_f') concept [35]. For our measurements, T_f' is defined as the temperature of intersection of the extrapolated equilibrium liquid and glass $\Delta(T)$ curves. T_f' is computed directly from $d\Delta/dT(T)$ dependencies; corresponding geometric construction is described elsewhere [23].

To prevent sample contamination, oxidation, and moisture uptake, all measurements are performed in high oil-free vacuum (about 10^{-7} torr). A liquid nitrogen trap is situated in the vicinity of the sample to further reduce moisture sorption on the sample. The ionization vacuum gauge remained off during the entire temperature scan series to prevent sample damage.

B. Sample preparation

Two types of monodispersed atactic polystyrene, abbreviated as PS-212k ($M_W = 212$ kg/mol, $M_W/M_N = 1.05$) and PS-9M ($M_W = 8990$ kg/mol, $M_W/M_N = 1.22$), were purchased from Polymer Source, Inc., and used for the most of the experiments. Prime-grade low-doped Ø 51 mm silicon wafers (>1 Ω cm resistivity, 0.26–0.31 mm thickness, ⟨100⟩ orientation, Montco Silicon Technologies, Inc.) were typically used as substrates. Some of the experiments described at the end of the discussion section (summarized in Fig. 11) use different PS and substrates; the differences are specified in the discussion section where appropriate. The PS coatings were formed by the spin-cast method from PS solutions in ACS reagent grade toluene with >99.5% purity and <10 ppm residue upon evaporation (Sigma-Aldrich), at 3000 rpm for 60 s. Two coating procedures were utilized. Following one procedure, the coating was performed in a class 100 clean room environment. The solution was filtered through a 0.2 μm PTFE syringe filter right before deposition. The other procedure assumed no filtration; a spin coater was situated in a regular wet chemistry lab. Solutions were prepared and kept in chemically inert Teflon FEP bottles with Tefzel ETFE closures. Silicate glass was the only other material that was in contact with the solvents and solutions. All chemicals and plastic and glass labware used in the preparation were dedicated for this project only and kept separately.

Before coating, the substrate surface was cleaned in oxygen plasma for 10 min (PE-200 Oxygen Plasma Surface Treatment and Etching System, 250 W RF power, 50 cm^3/min oxygen gas flow). For some experiments, Si substrates with hydrogen-terminated (H-terminated) surface were fabricated following the procedure described elsewhere [36]. After oxygen plasma cleaning, a wafer was immersed in 40 wt.% aqueous solution of NH_4F (certified ACS grade, Fisher Scientific) for 6–7 min, followed by thoroughly rinsing in deionized water and drying with nitrogen. The NH_4F solution dissolves the native oxide layer and a layer of Si-H groups is formed on the surface. The hydrophobicity of the surface was tested after the preparation procedure by placing a small water droplet on the H-terminated surface and watching the shape of the droplet. The Si-H layer exhibits high stability to oxidation and hydrolysis. The H-terminated Si surface shows no sign of oxidation on air for several days and in water for about an hour [36]; coated by PS, the passivation layer is stable upon annealing at 150 °C in air [37]. The rms roughness of the H-terminated surface measured by AFM is 0.3 nm (rms) which is comparable with the rms roughness—0.2 nm—reported for Si(111) surfaces treated in a similar way [38].

Typically the sample preparation and *ex situ* characterization takes 1–2 h, immediately followed by placing the specimen in the optical vacuum chamber and evacuating for at least 1 day. Initial PS film thickness characterization was performed *ex situ* by an AutoElII-NIR-3 three-wavelength nulling ellipsometer (Rudolph Technologies, Inc.). Measurements also include ellipsometry on freshly cleaned substrates that yield the thickness of the native silicon oxide layer (1.5–2.0 nm typical). Additional characterization of the PS layer thickness in both *ex situ* and *in situ* conditions was performed by spectroscopic ellipsometry in the main experimental setup with a 460–1000 nm wavelength range. Thicknesses of the layers were calculated using the Film Wizard ver. 8.0.3 and FilmEllipse ver. 1.1 software packages (SCI). Selected samples were characterized by atomic force microscopy with a MultiMode MMAFM-2 system (Digital Instruments) in tapping mode. Nanoprobe SPM tips (type NP, wafer 113-149-2, Digital Instruments) were used.

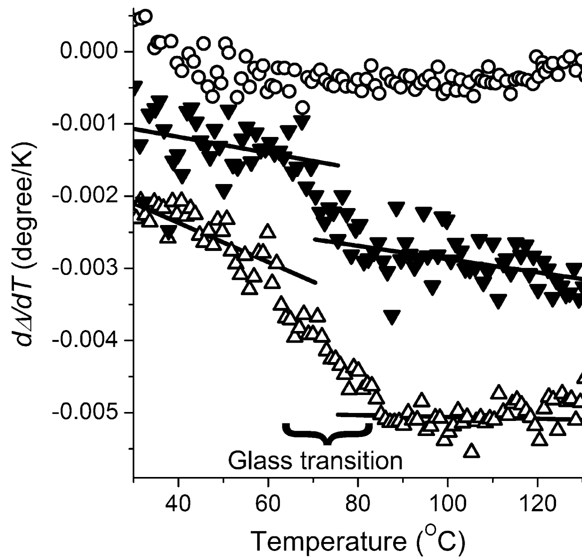

FIG. 1. Glass transition in 1–2 nm thick PS films. Open triangles represent data for a 1.2 nm thick PS-212k film on H-terminated Si obtained during linear heating run (average of 20 runs); the filled triangles represent data for a 1.4 nm thick PS-212k film on native silicon oxide surface obtained during TM cooling run (shifted up for clarity by 0.001°/K). Solid lines are the best fit for glassy and liquid state data points. Circles represent control data obtained for a clean native oxide surface during TM cooling run (shifted up for clarity by 0.0035°/K).

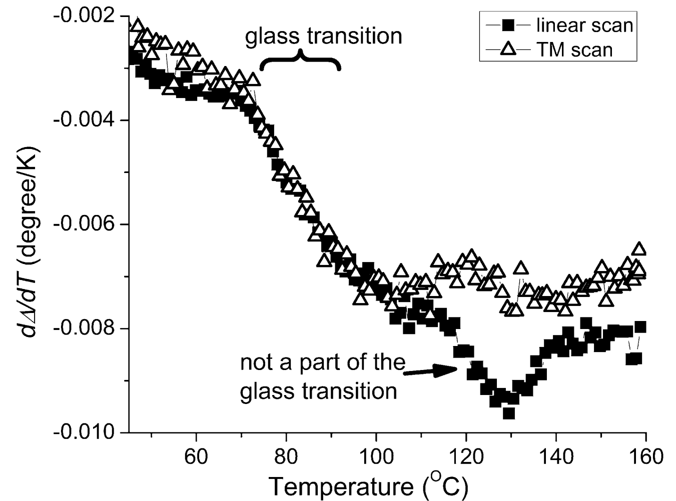

FIG. 2. Linear scan data (filled squares) in comparison with TM scan data (open triangles). Sample: 5.7 nm thick PS-212k coating on a native silicon oxide surface. Both curves are taken upon cooling. The linear scan curve is an average of 20 runs.

III. RESULTS AND DISCUSSION

The key advantage of the ellipsometry technique used in this work is a high sensitivity to thermal changes in a few nanometers thick coatings on a silicon surface. As a result, a clear observation of glass transition even in 1–2 nm thick PS films is possible; see Fig. 1. (It should be noted that at these thicknesses the coatings acquire significant roughness during the heat treatment, which is discussed below.)

To achieve this sensitivity, a clean controlled environment, extensive data accumulation, and advanced data processing are necessary. These factors are discussed in detail elsewhere [23]. It is worth noting that using ellipsometry is also advantageous from a sensitivity point of view. In general, if the polymer film becomes thinner, the signal from the sample weakens thus decreasing the signal-to-noise ratio. However, for the angle Δ measured by ellipsometry, this trend is partially compensated for by the nonlinear dependence of Δ on the film thickness h. For thin transparent layers on a silicon surface, the $d\Delta/dh$ slope increases drastically when h approaches zero [39]. A steeper slope means a larger response in Δ for the same thickness change caused by thermal processes. The magnitude of the effect can be illustrated by simple optical thin-film modeling using the Film Wizard software. The software shows that for a bare Si substrate at 70° angle of incidence and 504 nm wavelength, the $d\Delta/dh$ slope for 50 nm, 10 nm, and 1 nm thick PS coatings are 0.7°/nm, 2.9°/nm, and 3.5°/nm, respectively. Another practical consequence of this effect is that the signal strength can be increased further if the native silicon oxide layer on a substrate is partially removed. For example, the thickness of the oxide layer significantly decreases as a result of the H-terminated surface preparation procedure.

The temperature modulation (TM) technique is another key factor in reducing the experimental errors within our measurements. During a TM scan, the angle Δ is recorded while the sample temperature oscillates. In our case, TM effectively filters out irreversible thermal effects that can mask or alter the glass transition [33]. As is demonstrated below, both linear and TM scans yield comparable results both for T_g (Fig. 4) and other transition parameters (Figs. 6 and 8). However, the data processing of the linear scans is not fully independent from the TM-generated results. TM records are routinely used to verify the manifestation of the glass transition on the linear scans and to filter out masking features, thus greatly increasing the value of the linear scan results. The title of this work reflects this crucial role of the TM technique. The example of the transition clarification in a linear scan curve is given in Fig. 2. The linear scan data exhibit a peak at 115–140 °C that can be treated either as a part of the glass transition (the step in the 70–100 °C range) or as an unrelated effect. The absence of this feature on the TM scan curve suggests that the effect is not a part of the glass transition.

The method described above does not work if a spurious effect on a linear scan is superimposed over the glass transition. However, it is found that computing T_g out of the full cycle record, where both heating and cooling scans are averaged together, gives more dependable results. Figure 3 illustrates one of the worst linear scan experiments, where the glass transition on both heating and cooling scans is heavily disturbed. The difference between $T_g^{\rm Heat}$, obtained from the heating curve, and $T_g^{\rm Cool}$, computed from the cooling curve, achieves 22 °C. The shape of the full cycle curve is more regular and closer to the shape of TM scan shown for comparison on the same plot. $T_g^{\rm Cycle}$ computed from the full cycle curve is also close to the $T_g^{\rm TM}$ obtained by the TM method (the average of $T_g^{\rm TM}$ for all 6 TM scans for the same sample is

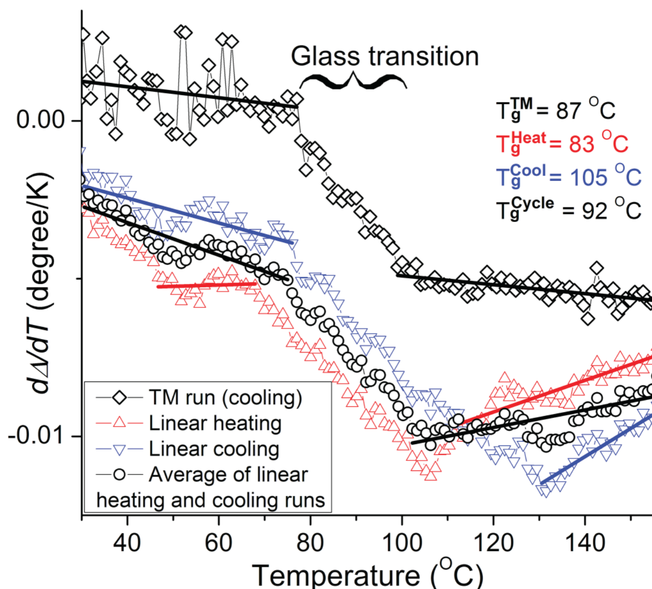

FIG. 3. (Color online) Linear scan data: red up triangles, blue down triangles, and circles denote heating scan, cooling scan, and full cycle, respectively. Second cooling TM scan (squares, shifted up by 0.001°/K for clarity) is shown for comparison. Solid lines are the best fits for glassy and liquid state data points. Sample: 9.2 nm thick PS-212k coating on a native silicon oxide surface. Both heating and cooling linear scan curves are averages of 20 runs. The full cycle curve is the average of both heating and cooling curves (average of 40 individual scans total).

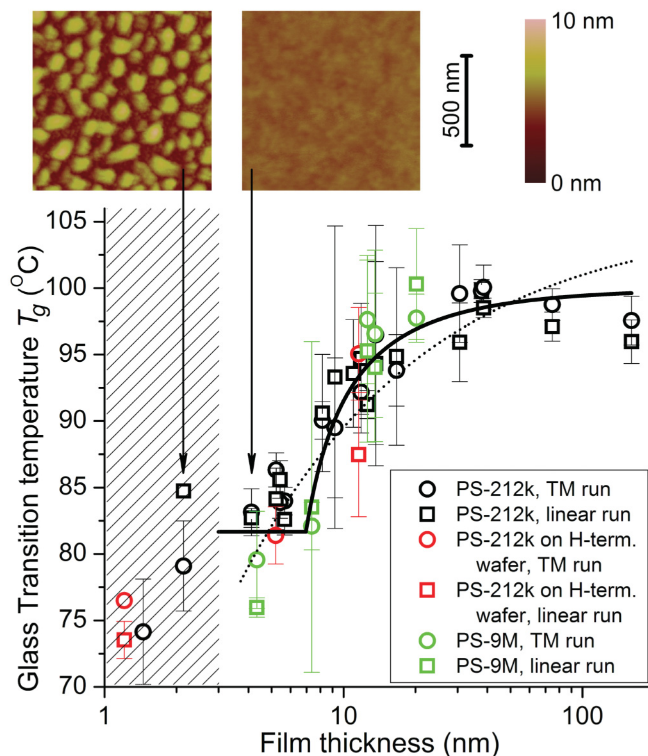

FIG. 4. (Color) Glass transition temperature as a function of PS film thickness. Data for PS-212k on Si wafers with native silicon oxide surface are shown in black, data for PS-212k on H-terminated Si wafers are shown in red, and data for PS-9M on Si wafers with native silicon oxide surface are shown in green. Circles and squares denote average T_g obtained from TM and linear scans, respectively. The averaging method is explained in the text. Error bars show standard deviation of the averaged T_g values. The thick solid black line is the two-layer model fit (see text). The dotted line is the best fit by Eq. (1). The hatching marks thickness range where significant surface roughening is observed. AFM images on the top are obtained for 2.1 nm and 4.1 nm thick PS-212k films (left and right images, respectively) on native oxide surfaces after all scans.

89 °C). The positive effect of the full cycle averaging can be explained by the existence of a factor that causes monotonic drift of Δ with time [23] (the drift rate and direction can depend on temperature). The heating and the cooling rates should be the same for this method to be effective. A working vacuum ionization gauge can cause this effect [23]; however, the gauge was off during all measurements described here. The nature of the effect requires an additional investigation. In our opinion, the full cycle averaging procedure can be considered as a primitive kind of temperature modulation technique: using a cyclic temperature program to filter out a specific type of irreversible process.

The composite plot of average T_g values for thin PS films supported by Si substrates as a function of film thickness is shown in Fig. 4. For TM measurements, the scans show reversible transition only, so T_g values found upon heating and upon cooling should be the same. Then, typically 3 T_g values from the individual heating scans and 3 T_g values from the cooling ones are averaged. For linear scan measurements, typically 21 cooling scans are averaged into a composite record, and $T_g^{\rm Cool}$ is computed from the record. Similarly, 20 individual heating scans yield the $T_g^{\rm Heat}$ value. The first heating run and the curves containing outliers are not taken into account. The common cause of the outliers is rapid changes of the air temperature in the laboratory affecting optical components and analog-to-digital conversion. Averaging heating and cooling composite records gives $T_g^{\rm Cycle}$, as described above. Finally, computing a numerical mean of $T_g^{\rm Cool}$, $T_g^{\rm Heat}$, and $T_g^{\rm Cycle}$ results in the average T_g value for the given linear scan experiment. A noticeable difference between $T_g^{\rm Cool}$ and $T_g^{\rm Heat}$ for some samples (as shown in Fig. 3) appears as relatively large errors of the linear scan values in Fig. 4.

There is a good agreement between temperature-modulated and linear scan experiments, on one hand, and between samples characterized by different PS molecular weights and PS/Si interfaces, on the other hand. Statistical tests (given in the Supplemental Material [34]) verify this agreement.

Figure 4 demonstrates that the T_g vs thickness dependence is not sensitive to some important sample characteristics. For high molecular weight PS (>200–300 kg/mol) M_W has no effect on T_g behavior, in agreement with many other studies [1,5]. In addition, the data on hydrophobic H-terminated surfaces and hydrophilic native silicon oxide surfaces overlap, suggesting that the nature of the polymer-substrate interface has a negligible effect on T_g even for a few nanometers thick films.

Before discussing the T_g dependence on thickness, it should be pointed out that the specimens with less than a three nanometer thick coating shown in Fig. 4 demonstrate pronounced surface roughening after experiment. The

roughening can be accounted for by dewetting of the PS coating. Three tested samples with thicknesses 2.1 nm, 1.5 nm, and 1.2 nm have rms roughness of 1.3 nm, 1.0 nm, and 0.7 nm, respectively. For comparison, typical rms roughness for coatings (both PS-212k and PS-9M) of four nanometers thick and thicker, as well as for films on a clean H-terminated Si surface, is 0.2–0.3 nm. Measurements on a clean Si surface typically show 0.1 nm rms roughness. It should be expected that $d\Delta/dT(T)$ dependencies are equally informative both for dewetted and continuous coatings. Optical characteristics of rough surfaces and interfaces (including discontinuous films) are well described by effective medium theories [39]. A dewetted film is approximated by an effective optical medium with certain thickness h_{EMA} and fraction of voids f_V. Effective index of refraction n_{EMA} is a function of f_V and the polymer's refractive index n. The form of the function corresponds to the specific effective medium model used. Index n, in turn, depends on the polymer's mass density ρ as expressed by the Lorentz-Lorenz equation. If the f_V value is constant, the thickness h_{EMA} is also determined by ρ. When the dewetting is over and the morphology of the film stabilizes, the $d\Delta/dT(T)$ curves reflect the temperature-induced changes in ρ that should be similar both for continuous and dewetted films. Accordingly, the step on the $d\Delta/dT(T)$ plots for the dewetted PS films (such as shown in Fig. 1) can be interpreted as the manifestation of the glass transition in the polymer "islands" on the substrate. However, since the islands have nonuniform thickness, T_g of the discontinued films are not directly comparable to the T_g of the flat coatings.

There is no meaningful change in T_g for PS films thicker than 20 nm. A slight decrease in T_g in comparison with the bulk value can be seen in the 10–20 nm range. Increased error bars mask this decrease in T_g. If the >10 nm thickness region would not be reliably accessible for our technique, we would have to acknowledge no appreciable dependence of T_g on PS film thickness. Substantial T_g depression becomes clear only for less than 10 nm thickness range. It is interesting that recent ellipsometric measurements made on comparable samples (PS with $M_W > 100$ kg/mol on a Si substrate) by other groups are in a good agreement with our results regarding the thickness range of the T_g depression effect. These groups report that the depression can be seen only for films less than 20 nm thick [8,15,40].

Perhaps the most intriguing characteristics of the T_g vs thickness dependence presented in Fig. 4 is an unusual steplike shape: While T_g decreases with thickness for more than 7–8 nm thick films, it stays nearly constant for thinner samples. Significant T_g dependencies reported in the literature are typically monotonic. Many studies fit the experimental T_g-thickness plots by the empirical equation proposed by Keddie *et al.* [26]:

$$T_g = f(h) = T_g^{\mathrm{bulk}}\left[1 - \left(\frac{A}{h}\right)^{\varepsilon}\right], \qquad (1)$$

where T_g^{bulk} is the glass transition temperature of the bulklike sample, A is a characteristic length, and ε is an exponent. The best fit of our data by (1) is shown in Fig. 4 by the dotted line. The best-fit parameters are $T_g^{\mathrm{bulk}} = 105.5 \pm 1.9\,^{\circ}\mathrm{C}$, $A = 0.03 \pm 0.02$ nm, and $\varepsilon = 0.55 \pm 0.08$. The fit exhibits excessive bulk T_g: The calorimetric value for the PS-212k sample is 99 °C [23]. The curve does not represent well the sharp T_g change in the 20–8 nm thickness range. However, the most prominent mismatch between the fit and the data can be seen for the thinnest samples. One of the interesting properties of the $f(h)$ function is that its slope increases with decreasing of thickness on the whole domain even in the semilogarithmic coordinates (as used in Fig. 4). Quantitatively, the difference $f(h) - f(h/2)$ is larger than the difference $f(2h) - f(h)$ by a factor of 2^{ε}. However, while T_g drops by about 10 °C on the 16 to 8 nm thickness interval, T_g stays practically constant for the 8–4 nm thickness range. This change of the $T_g(h)$ behavior at thickness of about 7–8 nm implies that (1) does not describe the presented data adequately.

We suppose that the increased sensitivity of our technique to thermal processes in films less than ten nanometers thick allows us to distinguish the flat portion of the T_g vs thickness function. To our knowledge, there is the only one source that reports the steplike T_g dependence on PS film thickness: Miyazaki *et al.* [25]. This historically first finding was made using a different technique, x-ray reflectivity measurements. However, the similarity between our results and the data reported by Miyazaki *et al.* is remarkable.

The simple two-layer model that was suggested by Miyazaki *et al.* for fitting the experimental T_g vs thickness dependence can be naturally adopted for our data. The two-layer model assumes that a supported PS film with thickness h in general consists of two distinct layers with thickness h_A and $h - h_A$ characterized by reduced and bulklike glass transition temperatures (T_g^- and T_g^{bulk}), respectively (see Fig. 5). The layer with reduced T_g^- has constant thickness h_A for thick films; films thinner than h_A contain no bulklike layer. Given this model the observable T_g can be calculated as a prorated average of T_g^- and T_g^{bulk}:

$$\begin{aligned} T_g &= \frac{h_A T_g^- + (h - h_A)T_g^{\mathrm{bulk}}}{h} \quad \text{for } h > h_A, \\ T_g &= T_g^- \quad \text{for } h \leqslant h_A. \end{aligned} \qquad (2)$$

To fit our data better, the contrast of the glass transition has been introduced to the model. This is the only improvement we have made for the model. The transition contrast δ in our case can be defined as a relative difference between $d\Delta/dT$

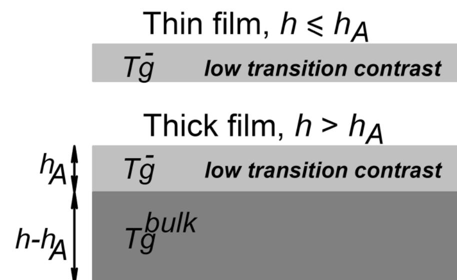

FIG. 5. Two-layer model for calculation of glass transition parameters for supported PS films of thickness h.

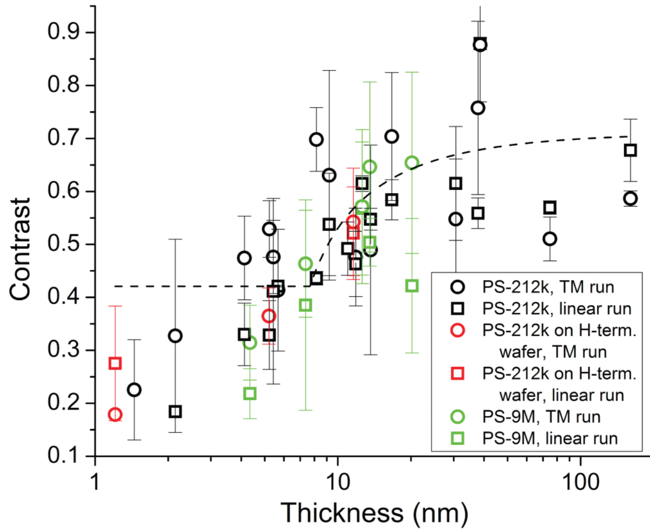

FIG. 6. (Color) Glass transition contrast as a function of PS film thickness. In correspondence with Fig. 4, data for PS-212k on Si wafers with native silicon oxide surface, data for PS-212k on H-terminated Si wafers, and data for PS-9M on Si wafers with native silicon oxide surface are shown in black, red, and green, respectively. Circles and squares denote transitions during temperature-modulated and linear scans, respectively. The averaging method is the same as used for T_g values shown in Fig. 4. Error bars show the standard deviation of the contrast values. The dashed line is two-layer model fit (given in the Supplemental Material [34]).

of liquid and glass, extrapolated to the T_g:

$$\delta = \frac{\frac{d\Delta^{\text{liquid}}}{dT}(T_g) - \frac{d\Delta^{\text{glass}}}{dT}(T_g)}{\frac{d\Delta^{\text{liquid}}}{dT}(T_g)}. \tag{3}$$

The loss of glass transition contrast as the film thickness decreases is a well-known phenomenon [1,2,17]. The loss of the contrast means that the difference between the glassy and liquid states vanishes. For our measurements, the loss of the contrast is illustrated in Fig. 6. To introduce the contrast δ in the two-layer model, we assume that the transition contrast for the reduced T_g layer is a fraction N of the bulklike transition contrast. The corresponding modification of (2) for the $T_g(h)$ function is

$$T_g = \frac{h_A N T_g^- + (h - h_A) T_g^{\text{bulk}}}{h + h_A(N-1)} \quad \text{for} \quad h > h_A,$$
$$T_g = T_g^- \quad \text{for} \quad h \leqslant h_A. \tag{4}$$

Note that Eq. (4) has four fitting parameters while Eq. (1) has only three of them. However, all the parameters in Eq. (4) have clear physical meaning, while constants A and ε in Eq. (1) are meaningless.

A standard nonlinear fit [41] of the experimental $T_g(h)$ curve (Fig. 4) yields all fitting parameters (T_g^-, T_g^{bulk}, h_A, and N) with reasonable precisions, despite the large amount of independent variables. This is expected, since different parts of the curve are sensitive to different parameters. Thus, asymptotic values at low and high thicknesses determine T_g^- and T_g^{bulk}, respectively; the position of the kink gives h_A; the range of thickness characterized by intermediate T_g decreases when N approaches zero. Table I compares our

TABLE I. Two-layer model parameters.

Parameter	Miyazaki *et al.* $M_w = 303$ kg/mol polystyrene	This work[a]
T_g^{bulk}	373 K	373.1 ± 0.6 K (99.9 ± 0.6 °C)
T_g^-	354.5 K	354.8 ± 0.2 K (81.7 ± 0.2 °C)
$T_g^{\text{bulk}} - T_g^-$	18.5 K	18.3 ± 0.6 K
h_A	8 nm	7.0 ± 0.4 nm
N	1	0.37 ± 0.12

[a]Fitting is performed using reciprocal square of T_g standard deviations of the data (shown as the error bars in Fig. 4) as weighting coefficients. Data points A-Q from Fig. 11 are merged with the data points shown in Fig. 4 for the final fit. Fitting procedure does not cover thicknesses less than 3 nm due to dewetting in the corresponding samples.

measurements with the results obtained by Miyazaki *et al.* [25] for $M_W = 303$ kg/mol PS.

Table I demonstrates good agreement for T_g depression amplitude ($T_g^{\text{bulk}} - T_g^-$) and the h_A parameter between two sets of data obtained by different experimental techniques. The difference in N seems not important: There are indications that the magnitude of the loss of transition contrast depends on the experimental method or/and parameters used for the glass transition monitoring [17]. Our measurements indicate that T_g for high molecular weight PS (PS-9M) fits the master curve (Fig. 4), while Miyazaki *et al.* obtained increased $h_A = 14$ nm for 2890 kg/mol PS. The nature of this discrepancy is not clear.

The data analysis technique employed in our work makes additional verification of the two-layer model possible. Examination of differential $d\Delta/dT(T)$ dependencies gives detailed information about the glass transition. For example, the transition width, existence, and characteristics of overshoot features and possible fine transition structure are readily accessible from the differential plots. In contrast, the simple and common method of glass transition characterization used by Miyazaki *et al.*—calculation of T_g as a temperature of the kink on the property versus temperature function—is far less informative.

The two-layer model implies that in the films where thicknesses of the bulklike and reduced T_g layers are comparable, a wider transition should be expected. Two transition steps of comparable magnitudes and shifted relative to each other will form a broad compound transition.

Numerically, the transition width value is computed using a normalized experimental $d\Delta^N/dT(T)$ function. Normalization means linear transformation of the $d\Delta/dT(T)$ curve so that $d\Delta^N/dT$ for glass state is equal to 0 and $d\Delta^N/dT$ for the liquid state is equal to 1. Then the transition width can be defined as the interval between the temperature when the $d\Delta^N/dT$ reaches some small value x ($0 < x < 0.5$) and the temperature when the $d\Delta^N/dT$ reaches $(1 - x)$ value. For x, we use values 0.1 and 0.25 and then the corresponding widths are denoted as $T_{0.8}$ and $T_{0.5}$, respectively. This procedure is illustrated in Fig. 7.

The dependence of $T_{0.8}$ on film thickness (Fig. 8) indeed shows elevated values in the 10–20 nm range. $T_{0.5}$

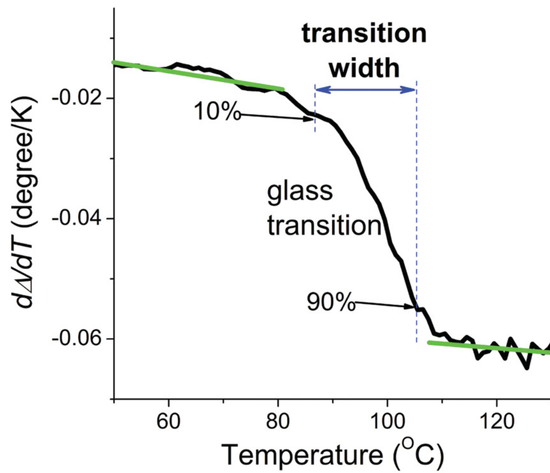

FIG. 7. (Color online) Definition of transition width. The sample is 160 nm thick PS-212k on Si/native Si oxide, linear cooling run.

demonstrates the same trend (shown in the Supplemental Material [34]). The transition width can be estimated using the two-layer model under some simplifying assumptions (corresponding formulas are given in the Supplemental Material [34]). The model values clearly reflect the broadening effect (Fig. 8).

In addition to the broadening of the transition, a few experiments demonstrate even stronger evidence for coexistence of two separate layers with different T_g: two resolved transition steps. An example is shown in Fig. 9: resolved transition steps in comparison with individual transitions in thin ($h < h_A$) and bulklike ($h \gg h_A$) films. Clearly, the low-temperature transition in the midsize film occurs at about the same temperature as the transition in the thin film, while

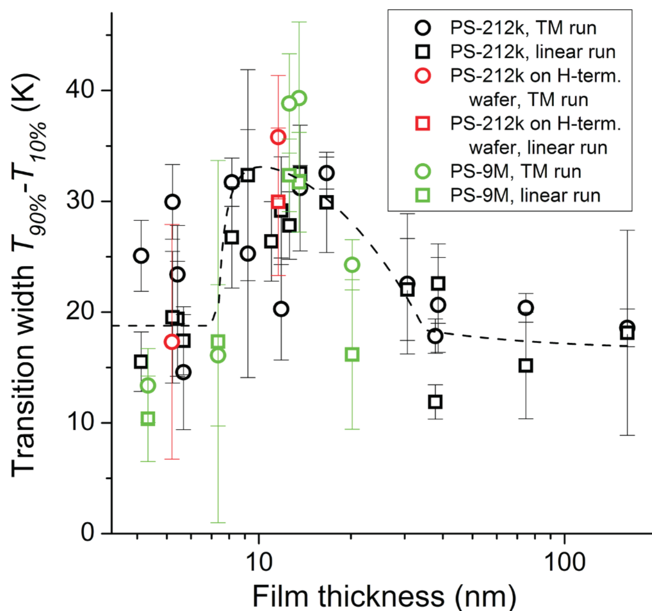

FIG. 8. (Color) Glass transition width $T_{0.8}$ as a function of PS film thickness. See Fig. 4 for symbol meanings. The averaging method is the same as used for T_g values shown in Fig. 4. Error bars show the standard deviation of the transition width values. The dashed line is two-layer model fit (given in the Supplemental Material [34]).

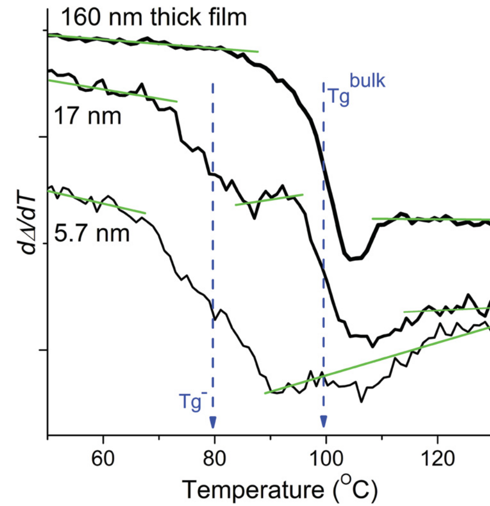

FIG. 9. (Color online) Two resolved glass transitions demonstrated by the linear heating scan of a 17 nm thick PS-212k film. Linear heating scans for 5.7 nm and 160 nm thick PS-212k samples are shown for comparison; they are vertically shifted for clarity. The curve for the thickest sample has a vertical scale 1:10. Each curve is the average of approximately 20 individual scans. The glass and liquid straight lines are guides for the eye.

the temperature of the high-temperature transition is close to the T_g in the bulklike film.

A double transition can be seen with more or less clarity for 12–20 nm thick films. The most distinct separation effect is found in the 13–17 nm thickness range. The effect is seen on all type of records: cooling, heating, and full cycle average curves. The conditions that should be met for clear observation of two separate transitions are narrow. The separation should not be significantly less than the sum of half-widths of both transitions. The magnitude of both transitions should be similar. In addition, linear scans are more suitable for resolution of two adjacent transitions than TM scans, because the temperature resolution of the TM technique is limited by the amplitude of temperature oscillations.

It is also worth noting that significant deviations in individual scans can imitate the transition separation observed in the average curves. Plotting all individual curves together is a good test to ensure that the transition separation effect is real: All meaningful features of the average curve should also be visible on the combined plot. Figure 10 demonstrates the combined plot of individual scans corresponded to the average curve with two separate transitions depicted in Fig. 9. The individual curves follow the common pattern formed by two separate transitions.

Interestingly, the existence of multiple glass transitions in thin PS films has been reported recently elsewhere, for both Si-supported [10] and freestanding [42] samples. Additionally, reduced T_g^- can be associated with faster segmental dynamics than the bulk. Stratified film structure with the high mobility layer at the free surface has been proposed by the Ediger group both for supported [9] and freestanding PS films [43]. The mobile layer thickness estimated from the fluorescent probe reorientation data is about 7 nm at T_g, in remarkable agreement with h_A obtained in our work.

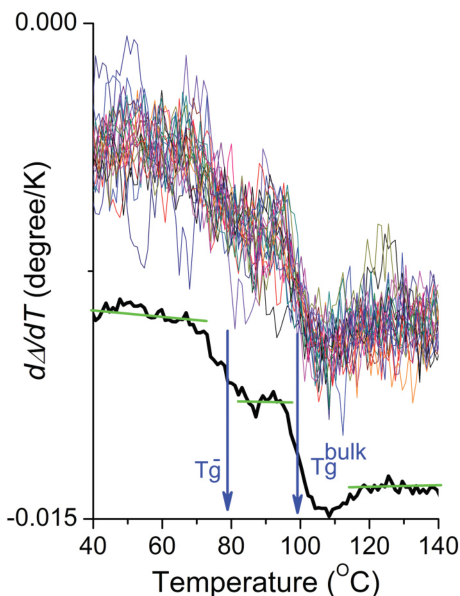

FIG. 10. (Color online) Individual linear heating scans for 17 nm thick PS-212k film and the average curve shifted down for clarity. The separation between two transitions on the average curve appears as a general trend in the individual curves. The glass and liquid straight lines are guides for the eye.

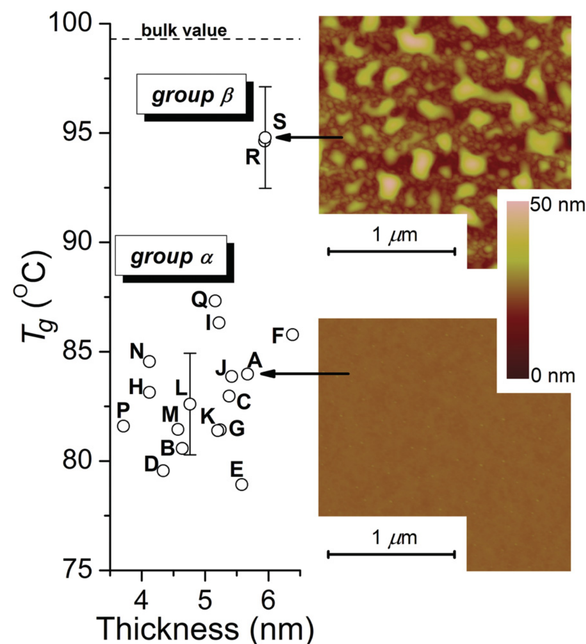

FIG. 11. (Color online) The plot on the left shows the influence of different experimental factors on the T_g depression effect. Data are obtained by the TM technique for PS coatings of about 5 nm thick; see text for the detailed description. Points are the averages of T_g values calculated from 6 (typically) TM scans. Error bars represent the standard deviation of the T_g values computed under supposition that the error distribution is the same for all measurements. Therefore, the error bars are the same for all data points. For clarity, the error bars are shown for selected points only. The dashed line denotes T_g for PS-212k in bulk samples by DSC [33]. The images on the right are AFM images of the surfaces of sample A (bottom image) and sample S (top image) obtained after all scans.

The sample preparation procedure can contain a hidden factor responsible for contradictory glass transition observations in thin films [44]. Insensitivity of the glass transition to the details of specimen pretreatment deserves additional analysis. Sample annealing effects on dynamics and glass transition in PS coatings have been discussed in detail recently [11,45,46], so this aspect of sample preparation is not covered here. However, it should be noted that no systematic changes in experimental curves for annealed samples have been noticed along the course of experiments. Altering the hydrophilic nature of the native silicon oxide surface by the H-termination procedure does not affect the glass transition, as mentioned previously. Also it should be mentioned that about one-quarter of the data points presented in Figs. 4, 6, and 8 are obtained from the samples fabricated under clean room conditions (see Sample Preparation section) while the rest of the samples are prepared in a regular wet chemistry lab. No differences were noticed between these groups of samples.

The effects of preparation techniques are examined in detail, using ≈5 nm thick supported PS films. These samples are thin enough to demonstrate significant T_g depression (about 18 K). At the same time, transition observation conditions for these films are far from the sensitivity limit (about 1 nm thick films) and ensure robust detection and characterization of the transition. Additionally, T_g in this thickness region is not sensitive to the variations in the sample thickness. Only the temperature modulation technique is used in these tests.

Several groups of experimental factors are examined and the results are summarized in Fig. 11. T_g of PS-212k film on a native oxide surface obtained under typical conditions is shown as data point A. As Fig. 11 demonstrates, T_g measured under different experimental conditions forms two groups of the data points on the plot. The group α surrounds data point A and the group β of data points are outliers. As a first approximation, we suppose that the experimental conditions that correspond to the data points of the group α demonstrate no influence on the T_g depression effect (within the error of measurement). Data points from the group β correspond to the conditions that significantly affect the T_g depression effect. Specific factors and the explanation for the deviation of the group β from the rest of the data are discussed below.

Polydispersity and manufacturer. The influence of the polydispersity factor (and PS manufacturer) is tested using medium molecular weight ($M_W = 289$ kg/mol) PS with a wide molecular weight distribution, $M_W/M_N = 2.2$, obtained from ACROS Organics. The corresponding data points B and C (Fig. 11) belong to the group α of data points: no noticeable effect of polydispersity and manufacturer on the T_g depression is observed. Also, the data point D obtained using PS-9M as a coating demonstrates no effect of high molecular weight on the T_g depression, as mentioned in the comments to Fig. 4.

Solvent contamination. Even miniscule contaminations in the solvent for spin-coating solutions can be disruptive for T_g measurements. For example, a typical weight fraction of PS in the solution for casting a 5 nm film is 0.2 wt.%. Reduction in T_g can be as high as 10 K for PS containing 1 wt.% of a plasticizer [47]. If the plasticizer is not volatile and stays in the film after pumping down and moderate heating, then its presence in the solvent at a 20 ppm level of concentration can reduce T_g of

the film by 10 K. Obviously, this T_g reduction effect vanishes for thicker films, since preparation of them requires solutions with larger PS concentration which have a lower plasticizer/PS ratio. This example demonstrates that the T_g depression effect in thin films can be caused by the insufficient solvent purity. The solvent impurity factor is addressed in several ways.

First, T_g in 5 nm thick PS film obtained using different solvents for spin coating, methyl ethyl ketone [48] and cyclohexane [49], are represented by the data points E and F in Fig. 11, respectively. They are close to typical T_g for this thickness (group α).

Second, increasing polymer concentration in the solution in conjunction with appropriately raising the velocity of spinning leads to films with the same thickness but reduced concentration of possible solvent contaminants. T_g of the film obtained from 0.3 wt.% PS solution in toluene cast at 10 000 rpm rotation speed (typical concentration is 0.2 wt.% and velocity is 3000 rpm) is represented by data point G in Fig. 11 and belongs to the group α.

Third, different toluene batches and grades are tested. Typically the toluene used for making polymer solutions in this work was ACS reagent grade [50]. Toluene from batch 69696EJ [51], batch 05296CK [52], and high-purity toluene [53] (last two solvents are taken from freshly opened bottles) were used for T_g measurements; see Fig. 11 data points H, I, and J, respectively. All of the data points are close to the typical T_g value (group α).

The fourth method of testing for solvent-induced depression is a concentration test. Evaporative concentration of very dilute PS solutions yields concentrated solutions with the same PS/low-volatile contaminant ratio. If the solvent contamination is the reason for T_g depression, thick films fabricated from the concentrated solutions should demonstrate the same T_g (depressed) as thin films fabricated from the initial (dilute) solutions. ACS reagent grade toluene from two different batches is used to make two 0.2 wt.% PS solutions. 5 nm thick PS films fabricated from these solutions show regular T_g depression; see Fig. 11, group α, data points H and I. These solutions are concentrated in an oil-free vacuum chamber by solvent evaporation up to the 1.2–1.4 wt.% of PS. 40 nm thick PS films fabricated out of the concentrated solutions demonstrate T_g values similar to the bulklike value, in agreement with the master curve shown in Fig. 4. The parameters of both experiments are given in Table II. All these experiments demonstrate that the solvent contamination factor is not responsible for the T_g depression effect in the experimental conditions of this work.

Surface treatment. First, as mentioned above, hydrogen termination of the silicon surface does not influence the glass transition. Data point K in Fig. 11 corresponds to a 5 nm thick PS film on H-terminated surface and belongs to the group α.

Second, the standard oxygen plasma cleaning procedure is replaced by a surface cleaning in a Nochromix wafer cleaning solution. A silicon wafer is immersed in a fresh mixture of 10.5 g of Nochromix (Godax Laboratories, Inc.) and 150 mL of concentrated sulfuric acid for about 20 h at room temperature. After a thorough rinsing of the substrate with deionized water and drying, it is subjected to the regular fabrication of a 5 nm PS film. The film demonstrates a regular T_g depression (data point L in Fig. 11, group α).

Third, to explore the insensitivity of T_g depression effect on the surface nature even further, a number of substrates with different metal coatings are prepared:

(1) 50 nm of Pt on 3 nm of Ti on 100 nm of SiN_X on 100 nm of SiO_2 on a Si wafer (Pt coating).

(2) 110 nm of Ti on a Si wafer (Ti coating).

(3) 80 nm of Au on 2 nm of Ti on a Si wafer (Au coating).

(4) 100 nm of Al on a Si wafer (Al coating).

(5) 120 nm of n-doped Si on an Al alloy substrate (Si coating on Al).

(6) Al alloy substrate (Al substrate).

Pt coating is identical to the metallization of sensors used in nanocalorimetry [54]. Ti, Al, and n-doped Si deposition are performed using CVC-601 DC Sputter Deposition System in argon atmosphere. CHA E-beam metal evaporator is used for Au/Ti deposition. Both deposition systems are located in a class 100 clean room. Prime-grade low-doped Ø 76 mm and Ø 100 mm silicon wafers, ⟨100⟩ orientation, were used as substrates for Pt, Au, Ti, and Al deposition. Polished aluminum alloy 6061 sheet, 0.8 mm thick, No. 8 mirror finish (McMaster-Carr part number 1655T11) is used as an Al alloy substrate. Ti-, Au-, Al-, and Si-coated substrates are used for PS spin-coating immediately after fabrication (within about 1 h) without any additional cleaning. Pt-coated substrates are soaked in acetone for several hours before spin coating. Al substrates are cleaned by soaking in toluene for several hours followed by oxygen plasma cleaning. The resulting surface has 4–5 nm thick native aluminum oxide layer (ellipsometry measurements), which is in agreement with literature [55]. Al substrates have visible polishing lines; all ellipsometry measurements on these substrates are performed so that the lines are parallel to the plane of incidence of the light beam.

Thin PS films on Pt, Ti, Au, and Si coatings show the typical T_g depression. Corresponding data points M, N, P, and Q in

TABLE II. Concentration test results.

Parameter	Experiment 1	Experiment 2
Toluene batch	[51]	[52]
PS thickness fabricated from initial 0.2% solutions	4.1 nm	5.2 nm
Concentration of the solutions after partial evaporation of the solvent	1.4%	1.2%
PS thickness fabricated from solutions after evaporation	39 nm	38 nm
T_g, TM method	100.1 ± 1.7 °C	99.8 ± 0.9 °C
T_g, linear temperature scans	98.5 ± 0.8 °C	99.8 ± 0.6 °C
T_g, expected from the master curve (Table I)	98.5 °C	98.5 °C

Fig. 11 belong to the group α. Similarity between T_g values obtained for Pt-coated and uncoated Si wafers agrees with the conclusion made by Fakhraai and Forrest [56] that the absence of significant T_g depression in nanocalorimetric experiments [17,18] on Pt-coated sensors is not a substrate effect. Using a Si-coated Al substrate instead of an uncoated Si wafer also has no effect on T_g. This indicates that T_g is not sensitive to the main composition of the substrate. Thin PS coatings on both Al and Al-coated substrates demonstrate T_g close to bulk values. Corresponding data points R and S in Fig. 11 form the group β. The deviation of the data points R and S from the rest of the points (group α) can be readily explained by the dewetting of the PS film on the native Al_2O_3 surface layer. An AFM image of the PS sample on the Al-coated Si surface after the experiment is shown as the inset in Fig. 11. The effective thickness of the PS in the droplets on the surface is significantly larger than the average film thickness, so T_g is close to the thick-film (bulk) values. It is worth noting that unusual large-amplitude depression of angle Δ is seen during the first heating of the samples (before annealing) on Al-coated Si substrates at the temperatures above glass transition. According to the effective medium theories discussed above, this process can be treated as an indication of the dewetting.

Summarizing, this section presents strong experimental evidence that the glass transition in 5 nm thick PS films does not depend on a wide range of experimental conditions. These conditions include polymer molecular weight, polydispersity, manufacturer, trace impurities in the solvent, substrate surface, and substrate material.

Two final remarks are appropriate here. First, there is a growing amount of evidences that a particular T_g behavior can be coupled to the type of film property probed in the measurement. For example, calorimetry measurements often report the absence of the T_g-thickness dependence, while probing thickness-related parameters (ellipsometry) usually yield noticeable T_g depression. It is worth noting that both nanocalorimetry reports [17,18] and this work have the same first author. Similar experimental habits, experience, and data processing techniques produce different T_g trends if applied to different experimental methods.

The time-scale argument becomes popular for explanation of the discrepancy in observed T_g vs thickness behavior [20,56,57]. It is hypothesized that the portion of the relaxation time spectrum probed in thin films at low frequencies is less dependent on temperature than the same portion of the spectrum in the bulk/thick film state. Oppositely, at high frequencies T_g does not depend on thickness [56,57]. However, this explanation does not make clear the nature of the thickness effect on T_g. Additionally, relaxation time–temperature maps used in this approach contain a point of singularity where dependencies for all thicknesses and bulk converge. The physical meaning of the characteristic time corresponding to the singularity (estimated as 2 s [56]) is not clear. An alternative explanation of the peculiar properties of an ultrathin supported film can be related to the residual stress in the coatings generated upon sample preparation [46,58]. However, this approach in regard to the glass transition in thin films has yet to be developed.

Second, no observable glass transition dependence for relatively wide PS thickness range (4–7 nm) can be of specific interest from the experimental point of view. According to the model, there is no stratification in these films; the layers of the coatings behave uniformly. Due to this property, 4–7 nm thick PS films can be convenient objects for the demonstration of confinement effects. At the same time, the properties of these unstratified coatings are not sensitive to variations in thickness (caused by preparation procedure). Therefore, the 5 nm thick coatings (with thickness from the middle of the mentioned thickness range) can be advantageous samples to study the dependence of thin film properties on a polymer and substrate characteristics and the details of sample preparation.

IV. CONCLUSIONS

Dependable characterization of the glass transition in thin glassy polystyrene films on silicon surfaces is performed by a state-of-the-art phase-modulated ellipsometry. The technique is advanced by using both linear and temperature-modulated temperature programs, extensive data accumulation, high-quality vacuum environment, and improved data processing methods. The reliable observation of the glass transition in 1–2 nm thick PS coatings has been achieved. The glass transition temperature T_g is found to be independent of film thickness and equal to the bulk value for films more than 20 nm thick. Thinner samples demonstrate unusual steplike T_g-thickness dependence, which is characterized by a constant T_g depression, about 18 K, for 4–7 nm thick films. This behavior can be readily explained by a two-layer model: PS coatings consist of a layer with bulklike properties and another limited thickness layer characterized by a depressed T_g. Despite the simplistic character of the model, it naturally explains unexpected phenomena of broadening of the transition in 10–20 nm thick films and a clearly separated double transition in some samples. It is also demonstrated that under standard laboratory conditions the T_g depression effect does not depend on a wide range of experimental factors, including molecular weight, polydispersity, manufacturer of the polymer, composition, surface, and pretreatment of the substrate, and type and specification of the solvent for spin cast.

ACKNOWLEDGMENTS

We thank Prof. Allen for supplying the Pt-coated substrates. This research is supported by the National Science Foundation through the Nanoscale Science and Engineering Center (DMR-0425880).

[1] J. A. Forrest, Eur. Phys. J. E **8**, 261 (2002).

[2] J. A. Forrest and K. Dalnoki-Veress, Adv. Colloid Interface Sci. **94**, 167 (2001).

[3] M. Alcoutlabi and G. B. McKenna, J. Phys. Condens. Matter **17**, R461 (2005).

[4] C. B. Roth and J. R. Dutcher, J. Electroanal. Chem. **584**, 13 (2005).

[5] O. K. C. Tsui, in *Polymer Thin Films*, edited by O. K. C. Tsui and T. P. Russell (World Scientific, Singapore, 2008), pp. 267–294.

[6] A. Serghei, Macromol. Chem. Phys. **209**, 1415 (2008).

[7] T. Kanaya, R. Inoue, K. Kawashima, T. Miyazaki, I. Tsukushi, K. Shibata, G. Matsuba, K. Nishida, and M. Hino, J. Phys. Soc. Jpn. **78**, 041004 (2009).

[8] M. Tress, M. Erber, E. U. Mapesa, H. Huth, J. Muller, A. Serghei, C. Schick, K.-J. Eichhorn, B. Voit, and F. Kremer, Macromolecules **43**, 9937 (2010).

[9] K. Paeng, R. Richert, and M. D. Ediger, Soft Matter **8**, 819 (2012).

[10] A. E. Ouakili, G. Vignaud, E. Balnois, J.-F. Bardeau, and Y. Grohens, Thin Solid Films **519**, 2031 (2011).

[11] S. Napolitano and M. Wübbenhorst, Nat. Commun. **2**, 260 (2011).

[12] V. M. Boucher, D. Cangialosi, H. Yin, A. Schönhals, A. Alegria, and J. Colmenero, Soft Matter **8**, 5119 (2012).

[13] S. Kawana and R. A. L. Jones, Phys. Rev. E **63**, 021501 (2001).

[14] K. Fukao and Y. Miyamoto, Phys. Rev. E **61**, 1743 (2000).

[15] A. N. Raegen, M. V. Massa, J. A. Forrest, and K. Dalnoki-Veress, Eur. Phys. J. E **27**, 375 (2008).

[16] V. Lupaşcu, H. Huth, C. Schick, and M. Wubbenhorst, Thermochim. Acta **432**, 222 (2005).

[17] M. Y. Efremov, E. A. Olson, M. Zhang, Z. Zhang, and L. H. Allen, Phys. Rev. Lett. **91**, 085703 (2003).

[18] M. Y. Efremov, E. A. Olson, M. Zhang, Z. Zhang, and L. H. Allen, Macromolecules **37**, 4607 (2004).

[19] W. E. Wallace, J. H. van Zanten, and W. L. Wu, Phys. Rev. E **52**, R3329 (1995).

[20] R. Inoue, T. Kanaya, K. Nishida, I. Tsukushi, M. T. F. Telling, B. J. Gabrys, M. Tyagi, C. Soles, and W.-l. Wu, Phys. Rev. E **80**, 031802 (2009).

[21] A. Serghei, M. Tress, and F. Kremer, J. Chem. Phys. **131**, 154904 (2009).

[22] B. D. Vogt, C. L. Soles, H.-J. Lee, E. K. Lin, and W. Wu, Polymer **46**, 1635 (2005).

[23] M. Y. Efremov, S. S. Soofi, A. V. Kiyanova, C. J. Munoz, P. Burgardt, F. Cerrina, and P. F. Nealey, Rev. Sci. Instrum. **79**, 043903 (2008).

[24] A. Serghei, H. Huth, M. Schellenberger, C. Schick, and F. Kremer, Phys. Rev. E **71**, 061801 (2005).

[25] T. Miyazaki, K. Nishida, and T. Kanaya, Phys. Rev. E **69**, 061803 (2004).

[26] J. L. Keddie, R. A. L. Jones, and R. A. Cory, Europhys. Lett. **27**, 59 (1994).

[27] G. B. DeMaggio, W. E. Frieze, D. W. Gidley, M. Zhu, H. A. Hristov, and A. F. Yee, Phys. Rev. Lett. **78**, 1524 (1997).

[28] T. Koga, N. Jiang, P. Gin, M. K. Endoh, S. Narayanan, L. B. Lurio, and S. K. Sinha, Phys. Rev. Lett. **107**, 225901 (2011).

[29] C. J. Ellison and J. M. Torkelson, Nat. Mater. **2**, 695 (2003).

[30] K. Paeng, H.-N. Lee, S. F. Swallen, and M. D. Ediger, J. Chem. Phys. **134**, 024901 (2011).

[31] C. White, W.-L. Wu, Y. Pu, M. Rafailovich, and J. Sokolov, Polym. Eng. Sci. **43**, 1241 (2003).

[32] C. White, K. B. Migler, and W.-L. Wu, Polym. Eng. Sci. **41**, 1497 (2001).

[33] M. Y. Efremov, A. V. Kiyanova, and P. F. Nealey, Macromolecules **41**, 5978 (2008).

[34] See Supplemental Material at http://link.aps.org/supplemental/10.1103/PhysRevE.86.021501 for examples of the raw data plots, description of statistical tests, and modeling of contrast-vs-thickness dependence and glass transition width.

[35] C. T. Moynihan, in *Assignment of the Glass Transition, ASTM STP 1249*, edited by R. J. Seyler (American Society for Testing and Materials, Philadelphia, 1994), pp. 32–49; I. M. Hodge, J. Non-Cryst. Solids **169**, 211 (1994).

[36] M. R. Houston and R. Maboudian, J. Appl. Phys. **78**, 3801 (1995).

[37] Y. Fujii, Z. Yang, J. Leach, H. Atarashi, K. Tanaka, and O. K. C. Tsui, Macromolecules **42**, 7418 (2009).

[38] N. Tomita and S. Adachi, J. Electrochem. Soc. **149**, G245 (2002).

[39] H. Fujiwara, *Spectroscopic Ellipsometry: Principles and Applications* (John Wiley & Sons, Ltd., Chichester, West Sussex, UK, 2007).

[40] Z. Fakhraai, S. Valadkhan, and J. A. Forrest, Eur. Phys. J. E **18**, 143 (2005).

[41] Origin 7.5 SR4 software, OriginLab Corp., http://www.OriginLab.com.

[42] J. E. Pye and C. B. Roth, Phys. Rev. Lett. **107**, 235701 (2011).

[43] K. Paeng, S. F. Swallen, and M. D. Ediger, J. Am. Chem. Soc. **133**, 8444 (2011).

[44] Y. P. Koh, G. B. McKenna, and S. L. Simon, J. Polym. Sci., B Polym. Phys. **44**, 3518 (2006).

[45] A. Raegen, M. Chowdhury, C. Calers, A. Schmatulla, U. Steiner, and G. Reiter, Phys. Rev. Lett. **105**, 227801 (2010).

[46] D. R. Barbero and U. Steiner, Phys. Rev. Lett. **102**, 248303 (2009).

[47] Z. Dong and J. R. Fried, Comp. Theor. Polym. Sci. **7**, 53 (1997).

[48] Methyl ethyl ketone, 99 + %, A.C.S. reagent grade, 25 ppm max. evaporation residue, Sigma-Aldrich 360473-500ML, batch No. 00952TC.

[49] Cyclohexane, certified A.C.S. grade, Fisher Scientific C556-500, lot No. 084512. Actual lot analysis: assay 99.9%, evaporation residue 0.0020%.

[50] Toluene, ⩾99.5%, A.C.S. reagent grade, 10 ppm max. evaporation residue, Sigma-Aldrich 179418-500ML.

[51] Toluene [44] batch 69696EJ, lot analysis: purity 99.94%, evaporation residue 0.000%.

[52] Toluene [44] batch 05296CK, lot analysis: purity 99.66%, evaporation residue 0.001%.

[53] Toluene Fisher Optima T291-4 for HPLC, pesticide residue analysis, GC, and spectrophotometry, lot 101346. Actual lot analysis: purity 99.99%, evaporation residue less than 0.1 ppm.

[54] E. A. Olson, M. Y. Efremov, M. Zhang, Z. Zhang, and L. H. Allen, J. Microelectromech. Syst. **12**, 355 (2003).

[55] H. Kang, K. Han, J.-E. Park, and H. H. Lee, Organic Electronics **8**, 460 (2007).

[56] Z. Fakhraai and J. A. Forrest, Phys. Rev. Lett. **95**, 025701 (2005).

[57] L. Hartmann, W. Gorbatschow, J. Hauwede, and F. Kremer, Eur. Phys. J. E **8**, 145 (2002).

[58] G. Reiter, M. Hamieh, P. Damman, S. Sclavons, S. Gabriele, T. Vilmin, and E. Raphaël, Nat. Mater. **4**, 754 (2005).